J. Plasma Physics (1999), *vol.* 61, *part* 5, *pp.* 671–699. Printed in the United Kingdom
© 1999 Cambridge University Press

Effective gravity due to the Hall effect and quasi-acoustic–gravity waves in accelerated plasma flows

LILIYA M. ALEKSEEVA

Institute of Nuclear Physics, M. V. Lomonosov Moscow State University, Moscow 117234, Russia

(Received 18 May 1998 and in revised form 10 November 1998)

The equations of resistive magnetohydrodynamics taking into account the Hall effect are solved analytically for the case of a planar plasma flow across the magnetic field. Waves of purely acoustic nature are revealed that propagate in the plasma medium on the background of a steady magnetically accelerated plasma flow of a rather arbitrary form. The magnetic field manifests itself in this process only in that it produces an effective gravity force, the 'gravitational' acceleration being proportional to $\omega_e\tau_e$. Like acoustic–gravity waves in the atmosphere, such quasi-acoustic–gravity (QAG) waves in a plasma can increase greatly in amplitude as they propagate 'upwards', i.e., in this case, counter to the direction of the electric field. In a plasma channel (where the plasma flows between the electrodes), a system of standing QAG waves arises, which has a stationary component. These waves are responsible for a number of distinctive features in the behaviour of Hall plasma flows, in particular for very large gradients and unexpected small-scale fluctuations of physical quantities near the anode, revealed earlier by numerical simulation. In the cases where the plasma-flow parameters provide a high intensity of these fluctuations, the flow appears to be unstable. In another range of parameter values, the QAG waves are strongly coupled with the electric currents that they induce in the electrodes, their amplitudes increase with time, and, again, the flow cannot be steady. The existence of a rather general dimensionless similarity criterion for resistive Hall plasma planar flows is also shown. This criterion can be found directly from the structure of the equations without any restrictions on the plasma parameters or on the form of the flow.

1. Introduction

In their pioneering work, Brushlinskiĭ and Morozov (1974) studied the establishment of plasma flows in the presence of the Hall effect. For accelerating channels, they revealed regimes in which the plasma flow, almost settled down to a steady state, exhibits sudden high-amplitude disturbances in the form of irregular oscillations in the neighbourhood of a certain point near the anode. Very sharp spatial non-uniformities and even a solitary explosion may be observed.

Although the role of the Hall effect in plasma dynamics has been actively studied in recent years (Holm 1987; Gordeev et al. 1994; Huba 1995), the physical nature

https://doi.org/10.1017/S0022377899007606 Published online by Cambridge University Press

of these phenomena has remained unknown up to now. It is the underlying physical mechanisms that are investigated in this study.

Brushlinskiĭ and Morozov (1974) numerically solved the equations of magnetohydrodynamics (MHD) with allowances made for resistivity and the Hall effect (i.e. RHMHD equations). This approach was applied to the investigation of isothermal axisymmetric flows accelerated transverse to the magnetic field in channels formed by solid (impermeable to ions), perfectly conducting electrodes of arbitrary profile. Three parameters enter into the set of equations considered: the characteristic ratio β of the gas pressure to the magnetic pressure, the magnetic viscosity ν (which is the reciprocal of the magnetic Reynolds number R_m), and the so-called exchange parameter ξ, which directly characterizes the Hall effect.

Brushlinskiĭ and Morozov regarded the principal result of their study to be the finding that the calculated flow reaches a steady state not for any value of the parameter ξ but only if $0 < \xi < \xi_{\rm cr}(\beta, \nu)$, where $\xi_{\rm cr}$ is a certain critical value. If, however, $\xi > \xi_{\rm cr}$ then, after a lapse of time, the solution experiences infinite growth in the vicinity of a certain point at the anode. A remarkable 'anode explosion' occurs in the form of pronounced decreases in density, plasma ejection from the this region, and the subsequent emergence of intense small-scale oscillations. Such a phenomenon is always found in numerical experiments for various channel geometries and different parameter values, being in any case observed at the anode. The critical ξ value determined from the numerical experiments can be approximated as

$$\xi_{\rm cr} \approx 0.3\beta^{1/4}\nu^{1/2} \tag{1.1}$$

(we use here the units adopted by Brushlinskiĭ and Morozov). Steady flows with the Hall effect ($\xi \neq 0$) exhibit a number of distinctions from steady flows at $\xi = 0$. The physical quantities are non-uniformly distributed across the flow. Their greatest gradients are observed near the anode, and at sufficiently large ξ a near-anode jump ('discontinuity') is formed. Plasma is pressed to the cathode, and this effect is the stronger, the smaller β and ν are. The electric current near the anode acquires a large longitudinal component, 'gliding' along the anode. As ξ approaches $\xi_{\rm cr}$, this 'gliding' current turns to the anode, thus forming a loop, or a 'vortex' of the current. At $\xi = \xi_{\rm cr}$ this results in the anode explosion.

Applied physics problems of obtaining steady flows, uniform in cross-section, turned the investigators' attention to searches for special means of suppressing the influence of the Hall effect on the flow. Subsequent research was mainly dedicated to the investigation of plasma flows in channels of complex design, basically with ion-current transport, where the plasma is injected into the channel not only through the channel inlet but also through electrode holes (see Brushlinskiĭ et al. 1979; Tereshin et al. 1990; Garkusha et al. 1992; Zimin and Morozov 1995; and references therein).

At the same time, Hall MHD itself is of substantial interest from a general physical standpoint, and its applications are numerous and diverse (see e.g. the review by Gordeev et al. (1994) and the review parts of the articles by Holm (1987) and Huba (1995)). In a natural plasma flow, the Hall effect could manifest itself in sharp flow non-uniformities and their dramatic growth, resulting in an unexpected solitary 'explosion' (for example, apparently similar features are observed in the breakup phase of a magnetospheric substorm in the near-Earth plasma convective flow (Alekseeva 1979)). In view of the aforesaid, investigation of the basic equations describing Hall plasma media is of paramount importance.

https://doi.org/10.1017/S0022377899007606 Published online by Cambridge University Press

We study here resistive Hall plasma flows by analytically solving the set of RHMHD equations considered by Brushlinskiĭ and Morozov (1974). In particular, (1.1) is obtained analytically for a rather wide range of plasma parameter values, the channel being assumed to be planar and of smooth profile. Specifically, in this case, if $\beta \to 0$, the solution can be written down for almost arbitrary values of ξ and ν (with $\xi/\nu = \omega_e\tau_e$) and, in fact, only the degenerate cases $\xi/\nu = 0$, $\nu/\xi = 0$ and $\xi = \nu = 0$ are excluded.

We find here the following interesting phenomenon. Against the background of a magnetically accelerated Hall plasma flow crossing a magnetic field, waves of purely acoustic nature can propagate, whereas the magnetic field manifests itself merely in producing an effective gravity force with a 'gravitational' acceleration proportional to $\omega_e\tau_e$. Just like acoustic–gravity waves in an atmosphere, such quasi-acoustic–gravity (QAG) waves in a Hall plasma increase greatly in amplitude as they propagate 'upward' (i.e. across the magnetic field, counter to the electric-field direction).

Rosenau et al. (1979) studied the nonlinear partial differential equations of MDH, making allowances for the Hall effect. They revealed real characteristics that show no trace of the fast, slow and Alfvén waves known in non-Hall MHD but describe sound waves absent in non-Hall MHD. The characteristic surfaces $\phi(\mathbf{r}, \mathbf{t}) = \text{const}$ are given by the equation $\mathbf{H} \cdot \boldsymbol{\nabla}\phi = 0$. The analysis did not take magnetic viscosity into account. The question of whether or not the corresponding system of basic equations is evolutionary has long been debated in the literature (Brushlinskiĭ and Morozov 1974; Rosenau et al. 1979; Holm 1987). Taking the magnetic viscosity ν into account imparts evolutionarity to these equations (Brushlinskiĭ and Morozov 1974). The existence of waves of acoustic nature in a Hall plasma, or QAG waves, revealed here for the case $\nu \neq 0$, confirms the conclusions of Rosenau et al. (1979).

The plan of this paper is as follows. In Sec. 2, we present the system of RHMHD equations and introduce the basic assumptions. In Sec. 3, we solve the equations for a plasma medium in an unbounded region and reveal the QAG waves. Then, in Secs 4–6, the more complex situation of plasma flow in a channel is considered. Section 4 takes into account the boundary conditions on the electrodes. As a result, the system of equations is reduced to a boundary-value problem for the QAG waves, which is then solved in Secs 5 and 6. Finally, the analytical results obtained for plasma channels are discussed in Sec. 7. In Sec. 8, we present certain generalizations for these results and clarify the physical sense of the basic constraints imposed on the parameters of the problem. The results of the study are summarized and certain considerations concerning laboratory experiments are discussed in Sec. 9.

At particular stages of this study, its preliminary results have been published in a number of papers (Alekseeva 1989, 1990, 1991, 1992a,b, 1993, 1994a,b, 1996).

2. Governing equations

According to Brushlinskiĭ and Morozov (1974), the set of HMHD equations in the commonly accepted notation has the following form:

$$\frac{\partial \rho}{\partial t} = -\boldsymbol{\nabla} \cdot \rho\mathbf{v}, \tag{2.1}$$

$$\rho\frac{d\mathbf{v}}{dt} = -\boldsymbol{\nabla}\mathscr{P} + \mathbf{j} \times \mathbf{H}, \tag{2.2}$$

https://doi.org/10.1017/S0022377899007606 Published online by Cambridge University Press

$$\mathscr{P} = \frac{\beta\rho}{2}, \tag{2.3}$$

$$\frac{\partial \mathbf{H}}{\partial t} = -\nabla \times \mathbf{E}, \tag{2.4}$$

$$\mathbf{E} = \nu\mathbf{j} - \mathbf{v} \times \mathbf{H} + \frac{\xi}{\rho}\left(\mathbf{j} \times \mathbf{H} - \frac{\nabla \mathscr{P}}{2}\right), \tag{2.5}$$

$$\mathbf{j} = \nabla \times \mathbf{H}, \qquad \nabla \cdot \mathbf{H} = 0, \tag{2.6}$$

where

$$\frac{d\mathbf{v}}{dt} \equiv \frac{\partial \mathbf{v}}{\partial t} + (\mathbf{v} \cdot \nabla)\mathbf{v}.$$

As the unit of length, we take an appropriately chosen characteristic scale l in the streamwise direction; for the units of density ρ and magnetic field H we take, the values ρ_* and H_* of these variables at some upper point (x_*, y_*) of the stream in the region under discussion at a time t_*. The Alfvén velocity $v_* = (H_*^2/4\pi\rho_*)^{1/2}$ at the mentioned point is adopted as the unit of velocity v, and the ratio of the unit of length to the unit of velocity, which is of the order of the transit time, serves as the unit of time t. Further, as the unit of the electric field $\mathbf{E}$ we take the quantity $H_* v_*/\hat{c}$ (where $\hat{c}$ is the speed of light), as the unit of the electric current j the combination $\hat{c}H_*/4\pi l$, and as the unit of pressure $\mathscr{P}$ the magnetic pressure $H_*^2/4\pi$. For simplicity and convenience in the comparison of our results with those of the numerical simulations by Brushlinskiĭ and Morozov (1974), we also assume the plasma to be isothermal; in this case, $\beta = 2c^2$, where $c = \text{const}$ is the gasdynamic speed of sound. For the same reason, the conductivity of the plasma λ_*, as well as its magnetic viscosity

$$\nu = \frac{\hat{c}^2}{4\pi\lambda_* l v_*} = \frac{1}{R_m},$$

are assumed to be constant. The exchange parameter

$$\xi = \frac{\hat{c}m_i}{el(4\pi\rho_*)^{1/2}}$$

(where m_i is the mass of an ion and e is the absolute value of the electron charge) characterizes the Hall effect, and is linked with the difference between the mean velocities of the ions and electrons by the relation

$$\xi\mathbf{j} = \rho(\mathbf{v}^i - \mathbf{v}^e).$$

Thus the plasma dynamics is determined by three constant parameters: β, ξ and ν (note that $\xi/\nu = \omega_e\tau_e$).

We introduce a Cartesian coordinate system (x, y, z) with the x axis directed in the streamwise direction and consider flows independent of z, of the form

$$\mathbf{v} = (v_x, v_y, 0), \qquad \mathbf{H} = (0, 0, H), \qquad \mathbf{E} = (E_x, E_y, 0). \tag{2.7}$$

For the chosen flow geometry, the equation $\nabla \cdot \mathbf{H} = 0$ is satisfied automatically, while the equation $\mathbf{j} = \nabla \times \mathbf{H}$ has the solution

$$\mathbf{j} = -\mathbf{e}_z \times \nabla H = \frac{\partial H}{\partial y}\mathbf{e}_x - \frac{\partial H}{\partial x}\mathbf{e}_y \tag{2.8}$$

(where $\mathbf{e}_x$, $\mathbf{e}_y$ and $\mathbf{e}_z$ are the unit vectors along the corresponding axes). Hence

https://doi.org/10.1017/S0022377899007606 Published online by Cambridge University Press

we obtain

$$\mathbf{j} \times \mathbf{H} = -\boldsymbol{\nabla}(\tfrac{1}{2}H^2).$$

The equation set (2.1)–(2.6) thus assumes the form

$$\frac{\partial \rho}{\partial t} = -\boldsymbol{\nabla} \cdot \rho \mathbf{v}, \tag{2.9}$$

$$\frac{d\mathbf{v}}{dt} = -\frac{1}{\rho}\boldsymbol{\nabla}\left(\mathscr{P} + \frac{H^2}{2}\right), \tag{2.10}$$

$$\mathscr{P} = c^2\rho, \tag{2.11}$$

$$\frac{\partial \mathbf{H}}{\partial t} = \nu\nabla^2\mathbf{H} + \boldsymbol{\nabla} \times (\mathbf{v} \times \mathbf{H}) + \xi\boldsymbol{\nabla}\frac{1}{\rho} \times \boldsymbol{\nabla}\frac{H^2}{2}, \tag{2.12}$$

$$\mathbf{E} = \nu\mathbf{j} - \mathbf{v} \times \mathbf{H} - \frac{\xi}{2\rho}\boldsymbol{\nabla}(\mathscr{P} + H^2). \tag{2.13}$$

We denote the solution of these equations as $\boldsymbol{\Pi}(x, y, t) = (\rho, \mathbf{v}, H)$ and seek it in the following form, which contains the independent variables only in certain specific combinations:

$$\boldsymbol{\Pi}(x, y, t) = \boldsymbol{\Pi}^0(x, y/\delta) + \tilde{\boldsymbol{\Pi}}(x, \gamma\delta x, y/\delta, \gamma y, \gamma c t). \tag{2.14}$$

Here $\boldsymbol{\Pi}^0$ is a known (background) steady-state flow with the characteristic transverse scale δ (the relation $v_y^0/v_x^0 \sim \delta$ being valid for its velocity components), $\tilde{\boldsymbol{\Pi}}$ is a varying deviation from this flow, and the gamma factor (Alekseeva 1980)

$$\gamma \equiv \gamma(\boldsymbol{\Pi}^0) = -\Gamma\left(\frac{H^0}{\rho^0}\right)^2 \frac{\partial H^0}{\partial x}, \qquad \Gamma \equiv \frac{\xi}{\nu c^2}, \tag{2.15}$$

characterizes the non-uniformity of $\tilde{\boldsymbol{\Pi}}$ in the transverse direction. We choose $\boldsymbol{\Pi}^0$ to be fairly uniform across the stream, so that

$$\frac{\partial \boldsymbol{\Pi}^0}{\partial y} \lesssim 1. \tag{2.16}$$

We assume that

$$c \ll 1 \qquad (\text{i.e. } \beta \ll 1). \tag{2.17}$$

Then, in the adopted units,

$$\frac{\partial \rho^0}{\partial x} \sim \frac{\partial H^0}{\partial x} \sim \frac{\partial v^0}{\partial x} \sim \rho^0 \sim H^0 \sim v^0 \sim 1. \tag{2.18}$$

We also put

$$\xi \gg c \gg \delta. \tag{2.19}$$

Hence, when (2.17) is taken into account, it is clear that we restrict ourselves to considering flows $\boldsymbol{\Pi}^0$ with smooth streamlines, so that

$$v_y^0/v_x^0 \sim \delta \ll 1. \tag{2.20}$$

The behaviour of $\tilde{\boldsymbol{\Pi}}$ will be studied for a time interval

$$0 \leqslant t \lesssim \frac{\delta}{c}. \tag{2.21}$$

https://doi.org/10.1017/S0022377899007606 Published online by Cambridge University Press

3. Travelling quasi-acoustic–gravity waves in a Hall plasma medium

Put

$$\frac{\xi}{c}\frac{\delta}{c} \gg \nu. \tag{3.1}$$

It follows from the conditions (2.19), (2.20), and (3.1) that

$$\Gamma\delta \gg 1, \qquad \Gamma \gg 1, \qquad \Gamma c \gg 1. \tag{3.2}$$

We assume that the differential operators acting on the quantity $\tilde{\Pi}$ change its order of magnitude in the following way:

$$\frac{\partial\tilde{\Pi}}{\partial x} \sim \Gamma\delta\tilde{\Pi}, \qquad \frac{\partial\tilde{\Pi}}{\partial y} \sim \Gamma\tilde{\Pi}, \qquad \frac{\partial\tilde{\Pi}}{\partial t} \sim \Gamma c\tilde{\Pi}. \tag{3.3}$$

Further, we assume that the quantities related to the field $\tilde{\Pi}$ are small, setting

$$\frac{1}{\nu\Gamma^2}\Phi(\Pi^0) \ll |\tilde{H}| \ll \min\left(\frac{1}{\Gamma\delta}, c^2\right), \tag{3.4}$$

where

$$\Phi(\Pi^0) \equiv \left|\nu\nabla^2\mathbf{H}^0 + \boldsymbol{\nabla}\times(\mathbf{v}^0\times\mathbf{H}^0) + \xi\boldsymbol{\nabla}\frac{1}{\rho^0}\times\boldsymbol{\nabla}\frac{(H^0)^2}{2}\right|. \tag{3.5}$$

Obviously, this is possible only if

$$\frac{1}{\nu\Gamma^2}\Phi(\Pi^0) \ll \min\left(\frac{1}{\Gamma\delta}, c^2\right), \tag{3.6}$$

which imposes one more restriction on the constant parameters ξ, ν, β and δ. This condition depends on the structure of Π^0. Note, in particular, that a solution I^0 of (2.9)–(2.13) for the case $\partial/\partial t = \xi = \nu = 0$ can be chosen as Π^0. Among such solutions I^0, there are isomagnetic streams ($H^0/\rho^0 = 1$), in which $\Phi(\Pi^0) = \nu|\Delta H^0|$. If an isomagnetic stream $\Pi^0 = I^0$ is, in addition, an iso-Bernoulli stream then $j_x^0 = \partial H^0/\partial y \sim \delta$ (see e.g. Alekseeva (1992a) and references therein) and $\Phi(\Pi^0) \sim \nu$. Hence the condition (3.6) is satisfied automatically, being merely a consequence of (3.2). In some cases, we shall deal with an isomagnetic, iso-Bernoulli background flow I^0, of the same β as assumed for Π, as with a simple and representative example of Π^0. It is known (Solov'ev 1963) that such flows greatly differ in the configuration of streamlines. Therefore the flows I^0 provide a good model for practically important streams.

The substitution of (2.14) into the x component of the Euler equation shows that if the terms nonlinear in $\tilde{\Pi}$ are small (as is actually the case) then

$$\tilde{v}_x \sim \max\left\{\frac{|\tilde{\rho}|}{\gamma c}, \frac{|\tilde{v}_y|}{\gamma c}, c\delta|\tilde{\rho}|, \frac{\delta|\tilde{H}|}{c}\right\}. \tag{3.7}$$

This relation allows us to conclude that the y component of the Euler equation reduces to

$$\frac{\partial\tilde{v}_y}{\partial t} = -\frac{1}{\rho^0}\left(c^2\frac{\partial\tilde{\rho}}{\partial y} + H^0\frac{\partial\tilde{H}}{\partial y}\right), \tag{3.8}$$

and the induction equation (2.12) integrated over y has the form

$$\frac{\partial\tilde{H}}{\partial y} = \frac{c^2}{H^0}\,\gamma(\Pi^0)\,\tilde{\rho} \tag{3.9}$$

(we assume the constant of integration to be zero). As a result, the order of $\tilde{H}$ with

https://doi.org/10.1017/S0022377899007606 Published online by Cambridge University Press

respect to $\tilde{\rho}$ is known. On taking (3.4) into account, we can check by the direct substitution of $\tilde{H}$ into the Euler equation that $|\tilde{\rho}| \ll 1$, $|\tilde{v}| \ll 1$, and the nonlinear terms of this equation are indeed small.

Equation (3.9) closes the gasdynamic part of the equation set. It is seen from (3.8) that in the situation at hand the electromagnetic processes generate a force proportional to $\tilde{\rho}$. In other words, the perturbation $\tilde{\Pi}$ 'feels' the effective gravitational force $g = -c^2\gamma(x, y)$ acting in the y direction.

Thus we now have to solve the obtained gasdynamic equation set. The above procedure of the comparison of the orders of magnitude reduces the continuity equation (2.9) to

$$\frac{\partial \tilde{\rho}}{\partial t} = -\frac{1}{\rho^0}\frac{\partial \tilde{v}_y}{\partial y}, \tag{3.10}$$

and the subsequent elimination of $\tilde{v}_y$ with the use of (3.8) and (3.9) gives

$$\frac{1}{c^2}\frac{\partial^2 \tilde{\rho}}{\partial t^2} = \frac{\partial^2 \tilde{\rho}}{\partial y^2} + \gamma(x, y)\frac{\partial \tilde{\rho}}{\partial y}. \tag{3.11}$$

This equation coincides in form with that describing acoustic–gravity waves propagating vertically in a neutral atmosphere (Lamb 1932; Hines 1960). In accelerated plasma flows, γ is positive and the upward direction in the atmosphere corresponds to the negative direction of the y axis (opposite to the predominant direction of the field **E**). The quantity $1/\gamma$ plays the role of the local scale height. The waves that propagate in plasma flows and are described by (3.11) are here called quasi-acoustic–gravity (QAG) waves. The acoustic nature of these waves with wavevector orthogonal to the magnetic field agrees with the conclusion of Rosenau et al. (1979) on the possibility of sound waves in Hall plasma media (see Sec. 1).

If γ does not depend on y (which is ensured, since I^0 is taken as Π^0), there exists a solution of the plane-wave type

$$\tilde{\rho} = \chi_A e^{-\gamma y/2} e^{i(\omega t - ky)} \tag{3.12}$$

(χ_A being the amplitude factor). When the wave propagates 'upwards', on passing the characteristic transverse scale δ of the stream Π^0, the amplitude of the wave increases by a factor $e^{\gamma\delta/2}$, where $\gamma\delta \gg 1$. In the case under consideration, the dispersion relation for QAG waves is $k^2c^2 = \omega^2 - \omega_L^2$, where $\omega_L = c\gamma/2$ is the lower frequency limit for travelling waves (the analogue of the Brunt–Väisälä frequency). The phase and group velocities of QAG waves are respectively $v_{\rm ph} = \omega/k = c/Q$ and $v_g = cQ$, where $Q = [1 - (\omega_L/\omega)^2]^{1/2}$.

When $\gamma(y)$ is variable, a wave of frequency ω should be reflected from the region where $\omega \approx \omega_L$. Consequently, there are reasons to make a technical recommendation: in order that QAG waves from a noise source do not break up the stream, one should choose a stream structure in such a way that the reflection region is 'upward' from the source, fairly close to it (we note that $\omega_L \propto \gamma(y)$).

In the case of variable $\gamma(y)$, the solution of (3.11) for the region far from the reflection regions can be found by the WKB method and has the form

$$\tilde{\rho} = (A_0 e^{i\omega(t-I)} + B_0 e^{i\omega(t+I)}) \exp\left(-\int \frac{\gamma}{2}\, dy\right),$$

where

$$I = -\frac{1}{c}\int Q\, dy,$$

A_0 and B_0 being arbitrary functions of x.

https://doi.org/10.1017/S0022377899007606 Published online by Cambridge University Press

QAG waves should be responsible for a peculiar phenomenon near the anode of an accelerating Hall plasma channel. A small perturbation can travel as a QAG wave, remaining unnoticeable, to the anode portion of the channel. Its amplitude increases exponentially, and, after a lapse of time, the perturbation will 'suddenly' manifest itself closer to the anode. If a set of QAG waves is present, such an *anodal burst* results in the development of irregular small-scale, high-intensity fluctuations near the anode. Fluctuations of this type were revealed in numerical simulations (see Sec. 1). The anodal-burst phenomenon in a plasma channel is an analogue of a well-known effect observed in the atmosphere: perturbations that were weak near the Earth's surface at $t = 0$ then travel upwards to result later in significant disturbances at the ionospheric level (Hines 1960).

4. Quasi-acoustic–gravity waves in a channel with sectioned conducting walls

A similar analytical solution (for the parameter domain extended to include $\Gamma\delta \sim 1$) can be obtained in the case of plasma flow in a channel bounded by the surfaces $y = R_1(x)$ and $y = R_2(x)$. These surfaces represent conductive walls, the anode and cathode respectively. We assume that they are smooth and that $s(x) = R_2 - R_1 \sim R_1 \sim R_2 \sim \delta \ll 1$. Let us specify the form of the channel walls, choosing them to be two stream surfaces of a known steady plasma flow $\mathbf{\Pi}^0$. As before, we seek a solution to (2.9)–(2.13) in the form (2.14).

4.1. Boundary conditions

We assume the walls to be impermeable to plasma ions, conducting and sectioned (Morozov and Solov'ev 1964; Brushlinskiĭ et al. 1979). The sections maintain a given electric-potential distribution, which specifies the corresponding tangential electric-field component E_p at the walls (here p is the variable measured along the electrode). Let $\mathbf{E}|_{\Pi^0}$ denote the right-hand side of (2.13) with $\mathbf{\Pi}$ substituted by $\mathbf{\Pi}^0$. We put $E_p = E_p|_{\Pi^0}$ on each of the channel walls.

Thus the boundary conditions for $\tilde{\mathbf{\Pi}}$ on the walls will be

$$\tilde{v}_n = 0, \qquad \tilde{E}_p = 0 \qquad \text{for} \qquad y = R_j \qquad (j = 1, 2), \tag{4.1}$$

where $\tilde{\mathbf{E}} = \mathbf{E} - \mathbf{E}|_{\Pi^0}$.

4.2. Adaptation of basic equations to the boundary-value problem

The imposition of boundary conditions leads to additional complications. In particular, the QAG waves can induce electric currents in the electrodes. The presence of the magnetic field of these currents can break down the second relationship in (3.3); as a result, it cannot be used for the comparison of the terms of the equations. Therefore we do not address immediately the simplified form of the basic equations and, when solving the problem, we retain the general form of these equations as long as possible.

We start by rearranging the original system (2.9)–(2.13) without imposing any restrictions on the parameters ξ, ν and β (in particular, we remove all of the restrictions introduced before).

Some of the terms in the equations of the initial system are products in which the factors are components of $\mathbf{\Pi}$ or their derivatives. When (2.14) is substituted into these terms, any product π of this kind is converted into a polynomial. Let us

https://doi.org/10.1017/S0022377899007606 Published online by Cambridge University Press

denote $\tilde{\pi} = \pi - \pi|_{\Pi=\Pi^0}$ and write $\tilde{\pi}$ in the form $\tilde{\pi} = \pi^l + \pi^N$, where π^l is the sum of the linear terms of the $\tilde{\Pi}$ components and π^N is the sum of the nonlinear terms. An expansion in powers of $\tilde{\rho}$ will be used for the terms of the equations that contain $\rho = \rho^0 + \tilde{\rho}$ in the denominator (in doing this, we do not necessarily assume $\tilde{\rho}$ to be small).

Let us choose I^0 as Π^0. On integrating (2.12) over y, we obtain

$$y(X_t' - \nu X_{xx}'') - \hat{\Phi}^0 - A + F\{Y_t'\} - F\{(\tilde{W}_y)_x'\} + \xi F\{h_y\tilde{\rho}_x' - (h_x)_y'(Y - \tilde{\rho}) - h_y\tilde{H}_x' + k^N\} = \nu\tilde{j}_x - \tilde{W}_x - \xi h_x(Y - \tilde{\rho}). \quad (4.2)$$

Here

$$\mathbf{W} \equiv \mathbf{v} \times \mathbf{B}, \qquad \mathbf{h} \equiv \frac{\boldsymbol{\nabla}\rho^0}{\rho^0}, \qquad \hat{\Phi}^0 = \nu F\{\Delta H^0\},$$

$$k \equiv -\left(\boldsymbol{\nabla}\frac{1}{\rho} \times \boldsymbol{\nabla}\frac{H^2}{2}\right)_z;$$

in accordance with the form of (2.8) for $\mathbf{j}$,

$$\tilde{H} = Y(x, y, t) + X(x, t), \qquad Y \equiv \int_{R_*}^{y} \tilde{j}_x \, dy, \quad (4.3)$$

$y = R_*(x)$ being an arbitrary curve ($R_1 < R_* < R_2$); a prime in combination with a variable written as a subscript denotes partial differentiation with respect to this variable; $F\{\ldots\}$ is some primitive in y (it will henceforth be convenient to assume that F denotes the integral from R_* to y); the constants of integration $A(x, t)$ and $X(x, t)$ must be found from the boundary conditions for $\tilde{E}_p$ (see (4.1)).

We notice that the group of terms forming the right-hand side of (4.2) enters through E_x into the expression

$$\tilde{E}_p = \tilde{E}_x + (R_j)_x'\tilde{E}_y \qquad (j = 1, 2). \quad (4.4)$$

We replace this group by the left-hand side of (4.2) and thus obtain a modified form of (4.4), which will be used later. Now we return to (4.2) and integrate it again over y to find

$$Z = \nu Y - F\{\tilde{W}_x\} - \xi F\{h_x Y\} + \xi F\{h_x\tilde{\rho}\}. \quad (4.5)$$

(The left-hand side Z of this equality will not be written out, because it is very cumbersome; however, it can easily be imagined from the form of the left-hand side of (4.2).)

Equations (4.4) in modified form and (4.5) constitute the basic equation set to be solved in what follows.

If $\delta \ll 1$, the components of $\Pi^0 = I^0$ are

$$\rho^0 = H^0 = \rho_0(x)[1 + O(\delta^2)], \quad (4.6)$$

$$v_x^0 = v_0(x)[1 + O(\delta^2)], \quad (4.7)$$

$$v_y^0 = \frac{1}{\rho_0}\frac{\partial G_0}{\partial x}[1 + O(\delta^2)], \quad (4.8)$$

$$G_0 = -\rho_0(x)v_0(x)[y - R_1(x)], \quad (4.9)$$

where G_0, ρ_0 and $\mathbf{v}_0$ are the lowest-order terms of the expansions of the stream function G^0, density ρ^0 and velocity $\mathbf{v}^0$ in powers of δ (see Morozov and Solov'ev 1974; Alekseeva 1992a; and references therein). The functions ρ_0 and v_0 of the single

https://doi.org/10.1017/S0022377899007606 Published online by Cambridge University Press

variable x are related by the Bernoulli equation $v_0^2/2 + \rho_0 = 1$ and the equation $\rho_0 v_0 s = -G_{0*} = \text{const}$. Thus the flow Π^0 is unambiguously determined if one of the three functions $\rho_0(x)$, $v_0(x)$ and $s(x)$ is given. We choose $s(x)$ to be given. Note that $j_x^0 = O(\delta)$.

4.3. Hierarchy of parameters revisited

Here we again introduce the relations (2.17), (2.19), (2.21) and (3.1), which ensured the existence of QAG waves in an unbounded medium. However, we now use the relation (3.1) in the less restrictive form

$$\frac{\xi}{c}\frac{\delta}{c} \gtrsim \nu. \tag{4.10}$$

Assuming $\tilde{\rho} \ll 1$, we seek a solution $\tilde{\Pi}$ that has the properties

$$\tilde{\Pi}'_x \sim \Gamma\delta\tilde{\Pi}, \qquad \frac{1}{\Gamma}\tilde{\Pi} \lesssim F\{\tilde{\Pi}\} \lesssim \delta\tilde{\Pi}, \qquad \tilde{\Pi}'_t \sim \Gamma c\tilde{\Pi}$$

(cf. (3.3)).

For the sake of simplicity, we exclude from consideration the points of the (ν, ξ) plane very close to the ν and the ξ axes (obviously, this does not lead to substantial losses in generality). Namely, we restrict ourselves to the region of the (ν, ξ) plane where

$$\nu \gg \frac{\delta}{c}, \qquad \frac{\xi}{\nu} \ll \frac{c}{\delta} \tag{4.11}$$

(and can approach the axes as closely as desired, choosing a sufficiently small value of c and then assuming $\delta \to 0$). A consequence of these inequalities,

$$\Gamma\delta c \ll 1, \tag{4.12}$$

will simplify our further calculations.

4.4. Procedure of solving the basic set of equations

In the basic set constituted by (4.5) and (4.4) in modified form, we neglect π^N, $\tilde{\mathbf{W}}$ and terms with $\hat{\Phi}^0$ (subsequently, we shall substitute the obtained solution into the basic set of equations in order to be sure that the omitted terms are small).†

As a result of this procedure, we obtain a system of three equations that determine the functions $Y(x, y, t)$, $X(x, t)$ and $A(x, t)$ in terms of the function $\tilde{\rho}(x, y, t)$, which we assume to be known. This system is greatly simplified thanks to the introduced hierarchy of parameters, so that (4.5) immediately determines $Y(x, y, t)$ in terms of $X(x, t)$ and $A(x, t)$. Then, on substituting the obtained expression for Y into the modified (4.4), the boundary condition $\tilde{E}_p = 0$ for either of the electrodes $y = R_j(x)$ becomes

$$\psi - A + \frac{\partial}{\partial x}\left[\frac{\xi}{\nu}A(R_j - R_*)\right] + (\xi h X - \xi X'_x) + [(R_j - R_*)X'_t] = 0 \quad (j = 1, 2), \tag{4.13}$$

$$\psi \equiv \frac{\xi c^2}{2\rho_0}\left(h\tilde{\rho} - \frac{\partial\tilde{\rho}}{\partial p}\right) + \frac{\xi^2}{\nu}\frac{\partial}{\partial p}\int_{R_*}^{y} h\tilde{\rho}\, dy, \tag{4.14}$$

($h = \rho'_{0x}/\rho_0$; for simplicity, we consider only such β that $b \equiv c^2/\delta = \beta/2\delta \lesssim \nu$).

† As can be seen from Sec. 3, the QAG waves are linear and their existence is not determined by the convective terms $\mathbf{W}$ or by the particular form of Π^0. The effects of interest must therefore be revealed from solutions $\tilde{\Pi}$ for which π^N, $\tilde{W}$ and $\hat{\Phi}^0$ are insignificant.

https://doi.org/10.1017/S0022377899007606 Published online by Cambridge University Press

Note that the third term (with A) of the left-hand side of (4.13) is of order $\epsilon_A A$, and the last term (with X) is of order $\epsilon_X(\xi hX - \xi X'_x)$, where

$$\epsilon_A = O\left(\frac{\xi^2\delta^2}{\nu^2 c^2}\right), \qquad \epsilon_X = O\left(\frac{c}{\xi}\right).$$

In the (ν, ξ) plane, we find the equality $\epsilon_A = \epsilon_X$ to be satisfied at the points of the curve

$$\xi = \xi^*(\nu) = c\left(\frac{\nu}{\delta}\right)^{2/3}. \tag{4.15}$$

In what follows, we study separately the regions in the (ν, ξ) plane that are situated below and above this curve.

4.5. The region below the curve (4.15)

Here $\epsilon_X > \epsilon_A$. When investigating this region, we retain only ϵ_X in (4.13), neglecting ϵ_A compared with unity. By subtracting (4.13) written for $y = R_1(x)$ from the same equation written for $y = R_2(x)$, we see that the equation

$$\tilde{E}_p\big|_{R_2} - \tilde{E}_p\big|_{R_1} = 0 \tag{4.16}$$

proves to have the form

$$sX'_t = -\psi|_{R_1}^{R_2}, \tag{4.17}$$

which yields

$$X = -\frac{1}{s}\int_0^t \psi|_{R_1}^{R_2}\, dt. \tag{4.18}$$

This leads to

$$Y = \frac{\xi}{\nu}\left[(y - R_*)(X'_x + hX) - \int_{R_*}^{y} h\tilde{\rho}\, dy\right]. \tag{4.19}$$

Thus $\tilde{H} = X + Y$ is known and can be substituted into the Euler and continuity equations to obtain the analogues of (3.7)–(3.11) (in doing this, it is convenient to make a comparison of values separately in two groups of terms of each equation: first between the terms with $\tilde{\rho}(x, y, t)$, and second between the terms with $X(x, t)$). Instead of the second relation in (3.3), we use the obvious estimate $\partial\tilde{\rho}/\partial y \lesssim \Gamma\tilde{\rho}$. Finally, we have

$$c^{-2}\tilde{\rho}''_{tt} = \tilde{\rho}''_{yy} + \gamma\tilde{\rho}'_y + \Theta(x, t), \tag{4.20}$$

whereas the first boundary condition (4.1) gives

$$\tilde{\rho}'_y + \gamma\tilde{\rho} = \theta(x, t), \qquad y = R_j(x), \tag{4.21}$$

where

$$\Theta \sim c^{-2}X''_{xx}, \tag{4.22}$$

$$\theta = \gamma h^{-1}(X'_x + hX) \sim \Gamma X'_x. \tag{4.23}$$

4.6. The region above the curve (4.15)

In this region, we have $\epsilon_X < \epsilon_A$ and neglect ϵ_X compared with unity in (4.13), retaining ϵ_A. After subtracting (4.13) written for $y = R_1(x)$ from the same equation written for $y = R_2(x)$, we obtain

$$\psi|_{R_1}^{R_2} + \frac{\partial}{\partial x}\left(\frac{\xi}{\nu}As\right) = 0.$$

https://doi.org/10.1017/S0022377899007606 Published online by Cambridge University Press

When calculating the function A, we substitute the result into (4.13) written for $y = R_1(x)$ and determine

$$X(x,t) = \frac{\nu}{\xi^2}\rho_0 \int_0^x \frac{dx}{\rho_0 s} \int_0^x \psi|_{R_1}^{R_2}\, dx \tag{4.24}$$

(we put $\tilde{\rho} = 0$ at the channel inlet). The function Y in this region proves to be the same as in Eq. (4.19). Finally, we find that density $\tilde{\rho}$ satisfies Eqs. (4.20) and (4.21) with

$$\Theta(x,t) \sim c^{-2} X'_x, \qquad \theta(x,t) \sim \Gamma X'_x. \tag{4.25}$$

4.7. Preliminary analysis of the boundary-value problem for $\tilde{\rho}$

To begin, we suppose that Θ and θ are small in some region of the (ν, ξ) plane. For this region,

$$c^{-2}\tilde{\rho}''_{tt} = \tilde{\rho}''_{yy} + \gamma\tilde{\rho}'_y, \qquad \left[\tilde{\rho}'_y + \gamma\tilde{\rho}\right]_{y=R_j(x)} = 0. \tag{4.26}$$

This equation has already appeared in the context of the unbounded medium (see (3.11)) and describes QAG waves. In the case of the unbounded medium, its solutions (3.12) have the scale $l_y \sim \Gamma^{-1}$ in the y direction. The boundary condition in (4.26) also points to the existence of the same scale. Hence we conclude that the solution of the boundary-value problem (4.26) has the same scale in the y direction. Therefore, in the region of (ν, ξ) plane where (4.26) are valid,

$$\int \tilde{\rho}\, dy \sim \frac{\tilde{\rho}}{\Gamma},$$

and, in accordance with (4.14), we can estimate $\psi \sim \xi\Gamma\delta c^2\tilde{\rho}$. Then (4.18) and (4.24) for $X(x,t)$ give

$$X \sim \xi c\tilde{\rho} \qquad \text{when} \quad \xi < \xi^*, \tag{4.27}$$

$$X \sim \tilde{\rho}(\Gamma\delta)^{-2} \qquad \text{when} \quad \xi > \xi^*. \tag{4.28}$$

Therefore the orders of magnitude of the quantities $\Theta\{\tilde{\rho}\}$ and $\theta\{\tilde{\rho}\}$ can be determined in the region where they are small.

Finally, on taking (4.19) into account, we find

$$\tilde{j}_x = \frac{\xi}{\nu}(X'_x + hX - h\tilde{\rho}), \tag{4.29}$$

with X included. The relations for v_x and v_y used above in the derivation of (4.20) and (4.21) now become

$$\frac{\partial \tilde{v_x}}{\partial t} = h\tilde{\rho} - X'_x - hX, \tag{4.30}$$

$$\frac{\partial \tilde{v}_y}{\partial t} = -\left(\frac{c^2}{\rho_0}\tilde{\rho}'_y + Y'_y\right). \tag{4.31}$$

4.8. The region Ω of the (ν, ξ) plane where free QAG oscillations exist

We begin with the region $\xi < \xi^*$. In the (ν, ξ) plane, we shall now locate the region Ω, where (4.26) are valid and free QAG oscillations exist. (In this subsection, we denote the solutions of (4.26) as $\rho^{(1)}$. These solutions will be found in Sec. 5, but now we already know that the function $\rho^{(1)}$ has the properties (3.3), which is sufficient to determine the configuration of Ω.)

https://doi.org/10.1017/S0022377899007606 Published online by Cambridge University Press

Let us compare (4.26) and (4.20) for the region Ω where Θ and θ (determined by (4.22) and (4.23) to order of magnitude) are small. We then vary the parameters ξ and ν, observing the respective changes in the values of Θ and θ. By composing the relations

$$\frac{\Theta}{\dfrac{\partial^2\rho^{(1)}}{\partial t^2}} \sim \frac{X'_x}{\rho^{(1)}\Gamma^2 c^2},$$

$$\frac{\theta}{\gamma\rho^{(1)}} \sim \frac{X'_x}{\rho^{(1)}} \gg \frac{\Theta}{\dfrac{\partial^2\rho^{(1)}}{\partial t^2}}$$

between the quantities Θ and θ and other terms of the equations in which they appear, we find that the influence of θ begins to manifest itself first.

Hence it turns out that the region Ω is adjacent to the region of the 'spoiled' boundary conditions in (4.26), i.e. to the region where, instead of (4.26), we have

$$c^{-2}\tilde{\rho}''_{tt} = \tilde{\rho}''_{yy} + \gamma\tilde{\rho}'_y, \qquad \left[\tilde{\rho}'_y + \gamma\tilde{\rho}\right]_{y=R_j(x)} = \theta(x,t). \tag{4.32}$$

with $\theta \cong \theta\{\rho^{(1)}\} \sim [\Gamma X\{\rho^{(1)}\}]'_x$. The solution of this boundary-value problem can be represented as $\tilde{\rho} = \rho^{(1)} + \rho^{(2)}$, where $\rho^{(2)} \ll \rho^{(1)}$, $\rho^{(2)}$ being associated with the inhomogeneity $\theta(\rho^{(1)})$ in the boundary condition. Obviously,

$$\rho^{(2)} \sim \frac{\theta(\rho^{(1)})}{\gamma} \sim X'_x\{\rho^{(1)}\}.$$

Hence, taking into account (4.27) for X, we can write

$$\frac{\rho^{(2)}}{\rho^{(1)}} \sim \frac{\xi^{\mathrm{I}}}{\xi},$$

$$\xi^{\mathrm{I}} \equiv \xi^{\mathrm{I}}(\nu,\beta) = \left(\frac{\nu}{\delta}\right)^{1/2}\left(\frac{\beta}{2}\right)^{1/4}$$

(we recall that $\beta = 2c^2$). Thus, as ξ approaches ξ^{I} from below, we see that the boundary of the region Ω of the existence of free QAG oscillations is specified by the curve

$$\xi = \xi^{\mathrm{I}}(\nu,\beta) = \left(\frac{\nu}{\delta}\right)^{1/2}\left(\frac{\beta}{2}\right)^{1/4}, \qquad \xi < \xi^*(\nu,\beta) \tag{4.33}$$

The same arguments can be applied to that part of the (ν,ξ) plane in which $\xi > \xi^*$ and (4.28) for X holds. As a result, we have the curve

$$\xi = \xi^{\mathrm{II}}(\nu,\beta) = \frac{\beta\nu}{2\delta}, \qquad \xi > \xi^*(\nu,\beta), \tag{4.34}$$

that specifies the lower boundary of the region Ω of free QAG oscillations. The boundaries of the region Ω are thus completely determined.

The region $\xi^{\mathrm{I}}(\nu,\beta) \leqslant \xi \leqslant \xi^{\mathrm{II}}(\nu,\beta)$, which does not belong to Ω, is indicated in Figs 1 and 2 by oblique hatching (for the case $\delta = 1/64$). Later, in Sec. 6, we shall return to this hatched area. Now it is only important that free QAG oscillations do not exist there.

To conclude this section, we estimate the values of the omitted terms of the basic set of equations. The omitted nonlinear terms are small only if the values of $\tilde{\rho}$ are sufficiently small, but the same $\tilde{\rho}$ values must be sufficiently large for the terms

https://doi.org/10.1017/S0022377899007606 Published online by Cambridge University Press

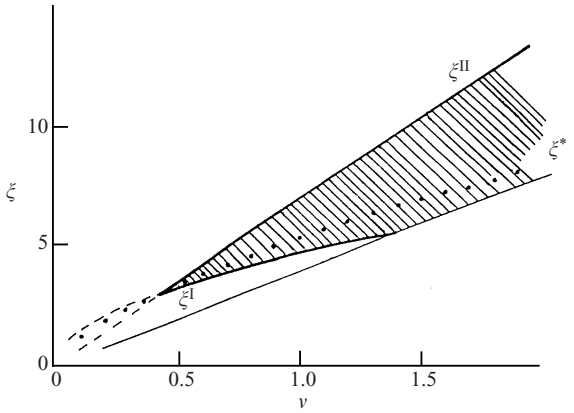


Figure 1. The region $\xi^{I}(\nu,\beta) \leqslant \xi \leqslant \xi^{II}(\nu,\beta)$ (oblique hatching) where steady-state solutions do not exist, for $b = \beta/2\delta = c^2/\delta = 7$, $\delta = 1/64$. See the text for details.

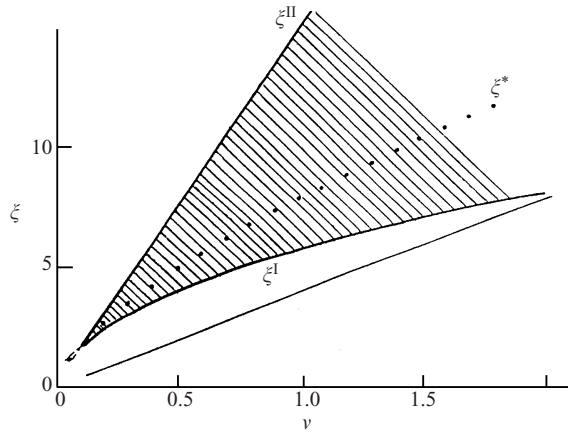


Figure 2. Same as in Fig. 1 but for $b = 15$.

with $\hat{\Phi}^0$ to be small compared with the linear terms. Equation (4.16), which was used to obtain (4.17) and (4.24) for $X(x,t)$, has the narrowest 'slot' in $\tilde{\rho}$, and is linear only for

$$\left(\frac{\nu}{\xi}\right)^2 \ll |\tilde{\rho}| \ll \frac{\xi\delta}{\nu} \tag{4.35}$$

(we recall that $\xi\delta/\nu \ll 1$ according to (4.11)), which, in turn, requires that

$$\xi \gg \nu\delta^{-1/3}. \tag{4.36}$$

The solution obtained is valid at points of the (ν,ξ) plane above the straight line $\xi = \nu\delta^{-1/3}$ (the light straight line in Figs 1 and 2).† The quantities $\tilde{\mathbf{W}}$ are small

† However, variations in $\tilde{\rho}$ associated with QAG waves should also exist below this line. Indeed, given the ν and the β values, for small ξ/ξ^{I} QAG oscillations are free or, in other words, independent of X. Consequently, the condition (4.36) of the linearity of the equation for X becomes unimportant in this region. Accordingly, the presumption of the electrically quasipotential nature of the process, which was used in earlier studies (Alekseeva 1990, 1992a,b) instead of the determination of X from the boundary conditions, does not affect the conclusion on the existence of free QAG waves obtained in these works.

https://doi.org/10.1017/S0022377899007606 Published online by Cambridge University Press

if $(\delta\nu/c)^{1/2} \ll \xi$. Taking into account the first relation (4.11), we see that this condition is satisfied automatically if (4.36) holds.

5. Free quasi-acoustic–gravity oscillations in a channel

In the region Ω of the (ν, ξ) plane where (4.26) are valid, $X'_x\{\tilde{\rho}\} \ll \tilde{\rho}$ (cf. (4.32)) and, in accordance with (4.29)–(4.31),

$$\tilde{j}_x = -\frac{\xi}{\nu} h\tilde{\rho}, \qquad \tilde{v}_x = h\int_0^t \tilde{\rho}\, dt + \tilde{v}_x(x, y, 0), \tag{5.1}$$

$$\tilde{v}_y = -\frac{c^2}{\rho_0}\int_0^t (\tilde{\rho}'_y + \gamma\tilde{\rho})\, dt + \tilde{v}_y(x, y, 0). \tag{5.2}$$

The boundary-value problem (4.26) assumes its simplest form

$$\tilde{\rho}''_{\tau\tau} = \tilde{\rho}''_{qq} + \tilde{\rho}'_q, \qquad \left[\tilde{\rho}'_q + \tilde{\rho}\right]_{q=q_j(x)} = 0 \tag{5.3}$$

in terms of the variables

$$\tau \equiv \gamma(x)ct, \qquad q \equiv \gamma(x)[y - R_1(x)] \tag{5.4}$$

($q = q_1 = 0$ corresponds to the anode and $q = q_2 = \gamma(x)s(x) = S(x)$ corresponds to the cathode). The variable x appears in the expressions as a parameter.

Seeking elementary solutions leads us to the eigenvalue problem

$$\Psi'' + \left(\Lambda - \frac{1}{4}\right)\Psi = 0, \qquad \left[\Psi' + \frac{\Psi}{2}\right]_{q=q_j} = 0 \tag{5.5}$$

for the function $\Psi \equiv U(q)e^{q/2}$. The complete orthogonal system of these functions is

$$\Psi_0(q) = a_0 e^{-q/2}, \qquad a_0 = \frac{1}{(1 - e^{-S})^{1/2}}, \qquad \Lambda_0 = 0, \tag{5.6}$$

$$\Psi_m(q) = \left(\frac{2}{S}\right)^{1/2} \cos(L_m q - Q_m), \qquad \Lambda_m = L_m^2 + \tfrac{1}{4}, \qquad m \geqslant 1, \tag{5.7}$$

where $L_m = \pi m/S$ and Q_m is determined by the relationships $\sin Q_m = (2\Lambda_m^{1/2})^{-1}$ and $\cos Q_m = -(L_m/\Lambda_m^{1/2})$. On this basis, we write down the solution of the boundary-value problem

$$\tilde{\rho} = e^{-q/2}\left[(M_0\tau + N_0)\Psi_0(q) + \sum_{m=1}^{\infty}(M_m \sin\omega_m\tau + N_m \cos\omega_m\tau)\Psi_m(q)\right], \tag{5.8}$$

$$M_0 = a_0\int_0^S M\, dq, \qquad N_0 = a_0\int_0^S N\, dq, \qquad \omega_m = \Lambda_m^{1/2}, \tag{5.9}$$

$$M_m = \frac{1}{\omega_m}\int_0^S (Me^{q/2})\Psi_m\, dq, \qquad N_m = \frac{1}{\omega_m}\int_0^S (Ne^{q/2})\Psi_m\, dq \tag{5.10}$$

for the initial conditions

$$\tilde{\rho}|_{\tau=0} = N(x, q), \qquad \left.\frac{\partial\tilde{\rho}}{\partial\tau}\right|_{\tau=0} = M(x, q), \tag{5.11}$$

N and M being arbitrary functions of the variables x and q. We assume that at $t = 0$

https://doi.org/10.1017/S0022377899007606 Published online by Cambridge University Press

the velocity $\tilde{\mathbf{v}}$ is such that the flux through the cross-section does not vary along the channel. Then $M_0 = 0$. This sort of initial conditions can give rise to only a steady zeroth mode and to a superposition of harmonic oscillations with time-independent amplitudes. In view of this, if $\tilde{\Pi}$ is considered to be a perturbation of Π^0 then the background stream Π^0 can be regarded as being stable against QAG-wave-type perturbations (although this stream Π^0 was not necessarily chosen to be a solution of the original system of equations). For large S, however, this conclusion may be of academic interest, because, if the initial perturbation involves the cathode zone, the amplitudes of harmonic oscillations can be very large near the anode. We shall discuss this point in more detail below.

We see that the steady zeroth mode of density perturbations is proportional to $P = e^{-q}$. It should be noted that, according to (5.2) and (5.1), the corresponding term $\tilde{v}_{y0}$ is zero whereas $\tilde{v}_{x0}$ grows linearly with time. But the values of $\tilde{v}_{x0}$ are much less than the values of $\tilde{\rho}$; therefore, if we are not interested in the behaviour of $\tilde{v}_{x0}$, we can treat the flow with $\rho = \rho^0 + N_0\mathrm{P}$ as being steady. If the second of the relations (4.11) is taken into account, the first equation in (5.1) shows that, even for the lowest possible values of $\tilde{\rho}$ permitted by (4.35), we have $\tilde{j}_{x0} \gg \delta/c$. This electric current perturbation greatly exceeds the background current component $j_x^0 \sim \delta$. Hence we find that the electric current of the steady flow acquires a longitudinal component in the presence of the Hall effect. This conclusion is in agreement with the data from numerical simulations (see Sec. 1).

Let us consider the general case in which other eigenmodes are also present. We see from (5.8) that $\tilde{\rho}$ is determined by the single parameter $S(x)$, which is the ratio of the channel depth $s(x)$ to the Hall y-inhomogeneity scale $l_y = \gamma^{-1}(x)$. This S dependence is striking. For S less than or about unity, only weak, incomprehensible 'ripples' of $\tilde{\Pi}$ are present against the background of Π^0. If S is large enough, exotic features of the Hall-plasma flows can be observed. We describe these now.

The zeroth mode of $\tilde{\rho} \propto P$ vanishes in the cathode zone of the channel and forms a jump (a very large transverse gradient) near the anode, the depth of this region being of the order of l_y. In accordance with (5.1), the longitudinal current perturbation component $\tilde{j}_{x0}$ manifests itself only within this very thin layer near the anode. Thus a steady flow with $\rho = \rho^0 + N_0 P$ appears to be significantly non-uniform in y, and its structure agrees with the results of the numerical simulations in its dependence on the parameters ξ, ν and β (see Sec. 1).† As for $\tilde{v}_{x0}$, this perturbation also proves to be concentrated in this layer next to the anode, forming an anode jet.

At large S, the amplitudes of oscillations near the anode are also much greater than near the cathode. In contrast to the amplitude of the zeroth mode of $\tilde{\rho} \propto P$, these oscillation amplitudes prove to be very sensitive to the y distribution of the initial perturbations (5.11) because of the presence of the weight function in the integrals (5.10). As a result, an initial perturbation localized within the anodal-jump layer or near it gives rise to relatively weak disturbances, which remain localized in the vicinity of the anode. But an initial perturbation that involves the cathode zone results in extremely intense fluctuations near the anode. In other words (cf. Sec. 3), the anodal burst occurs for large S in a channel with the cathode zone perturbed.

† An analytical study of the steady-state Hall flow in a quasi-one-dimensional channel was carried out for a similar formulation of the problem by Morozov and Shubin (1965). They investigated the case $\nu \ll \delta^2$, whereas here the case $\nu \gg \delta/c$, where $c^2 = \beta/2$ with $\beta \ll 1$, is considered.

https://doi.org/10.1017/S0022377899007606 Published online by Cambridge University Press

Now let us follow the evolution of the perturbation from its initial state until its breakdown into separate harmonics. We neglect the higher ($m > m_*$) insignificant terms of the series (5.8). Since taking M_m into account does not provide new information, we assume below that the velocity $\tilde{\mathbf{v}}(x, y, 0)$ ensures $M_m = 0$). We thus obtain

$$\tilde{\rho} \approx e^{-q/2} \left[N_0 \Psi_0(q) + \sum_{m=1}^{m_*} N_m \Psi_m(q) \cos \omega_m \tau \right]. \tag{5.12}$$

Accordingly, we have at $t = 0$

$$N(q) \approx e^{-q/2} \left[N_0 \Psi_0(q) + \sum_{m=1}^{m_*} N_m \Psi_m(q) \right]. \tag{5.13}$$

Let $\tau_{*\mu}$ denote the time needed to achieve a given difference μ between the phases of the harmonics with $m = 1$ and $m = m_*$ in (5.12).

We assume μ to be so small that the difference between $\cos \omega_m \tau$ and $\cos \frac{1}{2}\tau$ is negligible. Accordingly, it is evident from (5.7) and (5.9) for Λ_m and ω_m that if S is very large (as assumed) then $\tau_{*\mu}$ may be very large and may significantly exceed 4π. This means that, for a rather long lapse of time (up to $\tau_{*\mu}$), lower (the strongest) harmonics, while oscillating, remain in phase with one another; therefore

$$\tilde{\rho} \approx e^{-q/2} \left[N_0 \Psi_0(q) + \sum_{m=1}^{m_*} N_m \Psi_m(q) \cos \tfrac{1}{2}\tau \right], \tag{5.14}$$

or, in view of (5.13),

$$\tilde{\rho} \approx N_0 P(q)(1 - \cos \tfrac{1}{2}\tau) + N(q) \cos \tfrac{1}{2}\tau. \tag{5.15}$$

Thus we see a regime of coherent oscillations, in which the initial state and the state of anodal jump alternate. We can therefore call it the pulsating-anodal-jump regime. Since it may be the case that $|N_0| > |N(q)|$, the amplitude of the coherent oscillations may significantly exceed the initial perturbation $N(q)$. In the coherent-oscillation regime, $|\tilde{v}_x|$ determined by (5.1) increases in the anodal-jump layer in a stepwise manner, because the first term in (5.15) does not change sign with time. Therefore the value of $|\tilde{v}_x|$ becomes much greater than its initial value.

This regime of coherent oscillations breaks down after the moment $\tau = \tau_{*\mu}$ when the phases of individual harmonics cease to match one another and disordered small-scale fluctuations arise, whose amplitudes are maximum at the anode. This change in the regime is very sharp if the given perturbation $N(q)$ goes initially well beyond the anodal-jump layer. Then the coefficients N_m significantly exceed $N(q)$, N_0; therefore they also exceed the amplitude of the coherent oscillations (5.15). Fluctuations appear with progressively decreasing m and, accordingly, increasing amplitudes N_m. However, if an initial perturbation is present far from the anode, the amplitudes N_m of lower harmonics are so great that even a negligibly small difference between $\cos \omega_m \tau$ and $\cos \frac{1}{2}\tau$ should disrupt the regime of coherent oscillations at the very beginning of the process. Therefore this regime does not manifest itself.

Figures 3, 4 and 5 illustrate the behaviour of the density $\tilde{\rho}$ as established by solving (5.3) at $S = 50$. (The Laplace transform with respect to the variable t was employed, and, to perform the inverse transform, integrals were calculated numerically by the Gauss method (Alekseeva 1992b).) The initial perturbations are

https://doi.org/10.1017/S0022377899007606 Published online by Cambridge University Press

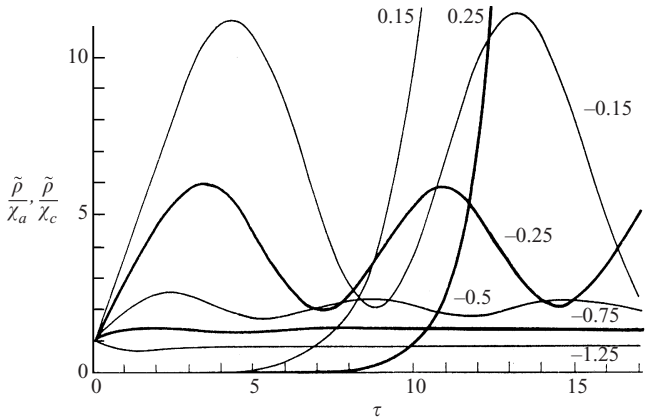


Figure 3. Temporal evolution of $\tilde{\rho}$ at the anode. The curves are labelled with the values of κ.

of the form

$$\tilde{\rho}|_{\tau=0} = N(x,q) = \chi(x)e^{\kappa q}, \tag{5.16a}$$

$$\left.\frac{\partial\tilde{\rho}}{\partial\tau}\right|_{\tau=0} = M(x,q) = 0. \tag{5.16b}$$

The thickness of the initially perturbed zone near the anode is different for different κ = const. (Here χ is an arbitrary function of x specifying the initial distribution of $\tilde{\rho}$ along the anode; in the figures, $\tilde{\rho}$ is normalized to χ_a (at the anode) and to χ_c (at the cathode) for $\kappa < 0$ and $\kappa > 0$ respectively.)

The obtained curves display all the above-discussed regimes of free quasi-acoustic–gravity oscillations. Figure 3 shows that the initial perturbation for $\kappa = -1.25$ (localized within the anodal-jump layer) produces only small $\tilde{\rho}$ in the subsequent evolution, whereas for greater values of κ the amplitudes of $\tilde{\rho}$ are greater. At the early stage of the process, we also see coherent oscillations in the anode zone of the channel ($\kappa < 0$).

Figure 4 illustrates the evolution of the perturbation $\tilde{\rho}$ for $\kappa = -0.25$ and for different values of η_1/s, where $\eta_1 = y - R_1(x)$. The perturbation was initially localized mainly in the anode zone, going, however, beyond the anodal-jump layer. Near the anode, the regime of coherent oscillations of moderate amplitude, or (which is the same) the regime of a pulsating anodal jump, is observed. After a lapse of time, it changes into the regime of intense, irregular high-frequency fluctuations. We can see that this is nothing other than the anodal burst (cf. Sec. 3). Before the anodal burst, small-scale fluctuations propagate as a 'cathode' wave of increasing amplitude (see Figs 4 and 5). In particular, as can be seen from Fig. 5, the cathode wave can acquire a wavepacket form in due course.

There is good reason to believe that the anodal burst is related to an unexpected 'anode explosion' in the almost-steady flow, which was observed in the numerical experiments (cf. Sec. 1). We can note the solitary character of both events, which are localized near a certain point at the anode (as is evident from our consideration, the localization point is the point of the maximum of $S(x)$). It is possible that the above-described increase of $|\tilde{v}_x|$ during the pulsating-anodal-jump regime results in the fact that, as can be inferred from Fig. 18 of Brushlinskiĭ and Morozov (1974), the longitudinal velocity substantially exceeds the transverse velocity at the mo-

https://doi.org/10.1017/S0022377899007606 Published online by Cambridge University Press

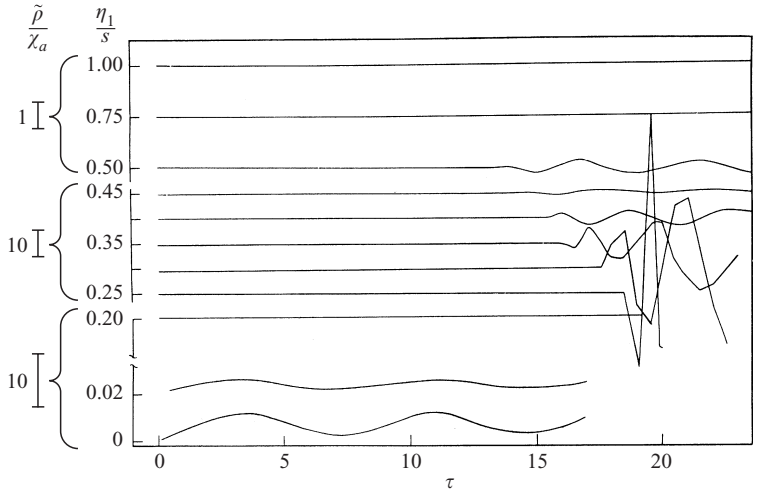


Figure 4. Time variation of the density perturbation (scaled according to the vertical bars) for $\kappa = -0.25$ and different values of η_1/s ($\eta_1/s = 0$ corresponds to the anode; $\eta_1/s = 1$ to the cathode).

ment of the anode explosion. Note that the solution of our linear problem (5.3) was found to within a constant factor, so that there is some uncertainty in the sign of the perturbation. However, in the case of near-anode perturbations, as shown qualitatively by Alekseeva (1980), nonlinear processes may eventually remove this indeterminacy. Below, in Sec. 6, we shall discuss in more detail the similarity between our results and the computational data of Brushlinskiĭ and Morozov (1974). Our formulae were obtained for ξ/ν satisfying the conditions (4.11) and (4.36) and for $\tilde{\rho}$ falling in the range (4.35). The peculiarities of the Hall plasma dynamics show up at very large S; therefore the question arises about the greatest value of S admissible in this conditions. It is clear that all the mentioned conditions are fulfilled if

$$\frac{\delta^{2/3}}{c^2} \ll S \ll \frac{1}{c}, \qquad \frac{e^S}{S^3} \ll \frac{c^6}{\delta^2} \tag{5.17}$$

Thus, if we choose an appropriate small value of c and then assume that $\delta \to 0$, we can consider arbitrarily large values of S.

In Fig. 6, the dotted area (which is part of the area of wavy hatching) corresponds to $S > 4$. The amplitude of each mode of free QAG oscillations is at the anode about seven times, or more, greater than at the cathode.

6. Interaction between free quasi-acoustic–gravity oscillations and currents induced by them in the channel walls

The curves $\xi = \xi^{\mathrm{I}}(\nu, \beta)$ and $\xi = \xi^{\mathrm{II}}(\nu, \beta)$ determined by (4.33) and (4.34) respectively, can be considered as conventional boundaries of the region Ω of free QAG oscillation (Figs 1 and 2). Near them, density perturbations satisfy (4.32). In Sec. 4, we sought solutions $\tilde{\rho} = \rho^{(1)} + \rho^{(2)}$ to these equations. Now, $\rho^{(1)}$ is determined by (5.8), and we can describe the properties of $\rho^{(2)}$ in detail.

Assume that

$$\rho^{(2)} = \frac{\theta(x,t)}{\gamma} + u(x,y,t) + r(x,y,t), \tag{6.1}$$

https://doi.org/10.1017/S0022377899007606 Published online by Cambridge University Press

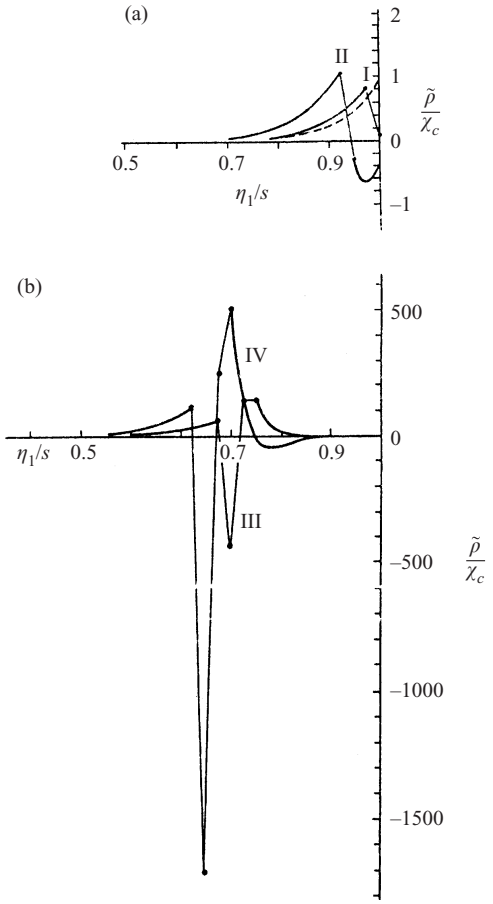


Figure 5. Cathode wave running from the cathode zone. The distribution of $\tilde{\rho}$ over the channel cross-section is shown for $\kappa = 0.25$ without fine details of sharp peaks: (a) $\tau = 0$ (dashed curve), 0.5 (I), 1.5 (II); (b) $\tau = 8$ (III), 9 (IV).

where u and r are the solutions of the auxiliary boundary-value problems

$$c^{-2}u''_{tt} = u''_{yy} + \gamma u'_y + \frac{\theta''_{tt}}{\gamma}, \tag{6.2}$$

$$u'_y + \gamma u = 0, \qquad y = R_j(x), \qquad j = 1, 2,$$

$$u|_{t=0} = u'_t|_{t=0} = 0$$

and

$$c^{-2}r''_{tt} = r''_{yy} + \gamma r'_y, \tag{6.3}$$

$$r'_y + \gamma r = 0, \qquad y = R_j(x), \qquad j = 1, 2, \tag{6.4}$$

$$r|_{t=0} = -\frac{\theta(x,0)}{\gamma}, \qquad r'_t|_{t=0} = -\left.\frac{\theta'_t}{\gamma}\right|_{t=0}. \tag{6.5}$$

Equations (6.3)–(6.5) turn out to coincide with the already-solved boundary-value problem (5.3) in the case of initial conditions (5.11) with N and M independent of q. The formula (5.10) shows that all eigenmodes are excited for such initial data. We see

https://doi.org/10.1017/S0022377899007606 Published online by Cambridge University Press

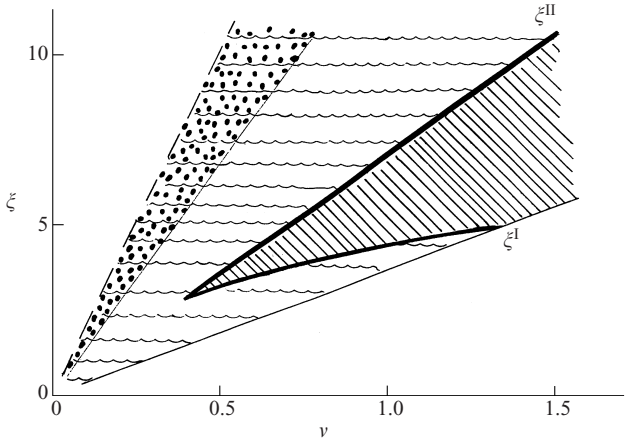


Figure 6. Regions of the manifestation of free QAG oscillations (wavy hatching), anodal burst (dotted), and current-exchange instability (oblique hatching), for $b = \beta/2\delta = c^2/\delta = 7$, $\delta = 1.75 \times 10^{-2}$.

immediately that the presence of $r(x, y, t)$ in (6.1) always ensures time dependence of $\rho^{(2)}$. Thus the considered boundary-value problem (4.32) has only time-dependent solutions.

Specifically, as ξ approaches $\xi^{I}(\nu, \beta)$ from below or $\xi^{II}(\nu, \beta)$ from above, the steady flow $\rho = \rho^0 + N_0 P$ with a steady-state anodal jump ceases to exist, and a transition to a non-steady-state regime takes place because of the presence of harmonic oscillations.

In addition, we note that in (6.2) for u the non-zero modes $\rho^{(1)}$ create a driving force θ''_{tt}/γ, whose frequencies correspond to the eigenvalues of the boundary-value problem. This resonance gives rise to an instability associated with the growth of $\rho^{(2)}$ with time.

As can be seen from a comparison of (4.26) and (4.32), the increase in the significance of the role of $X'_x\{\rho^{(1)}\}$ in the boundary conditions at the electrodes is responsible for the described change in the regime of QAG oscillations. We note that, according to (2.8), (4.19), (4.18), and (4.24), the electric current component $\tilde{j}_n = \tilde{j}_y - (R_j)'_x \tilde{j}_x$ normal to the electrode is equal to $\tilde{j}_n = -X'_x$. Correspondingly, an increase in X'_x with the approach of ξ to $\xi^{I}(\nu, \beta)$ from below or to $\xi^{II}(\nu, \beta)$ from above means an intensification of the exchange of currents between the plasma and the electrodes. This allows us to introduce, for the instability that manifests itself in this case, the term *current-exchange instability* of QAG waves in a Hall plasma flow.

It is worth noting a difference between the cases of ξ approaching $\xi^{I}(\nu, \beta)$ from below and of ξ approaching $\xi^{II}(\nu, \beta)$ from above. In the first case, the quantity X is represented by (4.18), and the expression for the driving force in (6.2) includes terms proportional to t^2, whereas in the second case we have (4.24) for X, and the expression for the driving force is a sum of periodic functions of t.†

† On taking into account the structure of (4.14) and (4.18), we can see that the quantity $\theta(x, t) \sim \Gamma X'_x$ is calculated by repeated differentiation with respect to x. Since the harmonic factors of the non-zeroth modes of $\rho^{(1)}$ contain x in the combination $\omega_m(x)\gamma(x)ct$, and (2.18) are valid, this procedure gives a multiplier as great as $\omega_m^2 \tau^2$. This is not the case if ξ approaches $\xi^{II}(\nu, \beta)$ from above, in which case, in accordance with the expression (4.24), the function X is determined by repeated integration with respect to x.

https://doi.org/10.1017/S0022377899007606 Published online by Cambridge University Press

Therefore the growth of small-scale fluctuations in $\rho^{(2)}$ with time is more dramatic if ξ approaches $\xi^{\mathrm{I}}(\nu)$ from below than if ξ approaches $\xi^{\mathrm{II}}(\nu)$ from above.

7. Stability of channel flows

A summary of the results of analytically solving the RHMHD equations for the channel flow is given in Fig. 6. The region $\xi^{\mathrm{I}}(\nu,\beta) \leqslant \xi \leqslant \xi^{\mathrm{II}}(\nu,\beta)$ where the current-exchange instability manifests itself is shown by oblique hatching for $b = \beta/2\delta = c^2/\delta = 7,\ \delta = 1.75\times10^{-2}$. Free QAG oscillations occur in region Ω (wavy hatching); in its dotted subregion, where the amplitudes of these oscillations are large, the anodal burst takes place ($S \geqslant 4$). As in Fig. 1, the light straight line is the lower boundary of the region where the channel solution is valid. The dashed straight line $\xi = c\nu/\delta$ reflects the simplifying limitation (4.11).

In the area where the amplitudes of QAG waves are small, the flow is stable (wavy hatching without dots). There are also two separate areas (wavy hatching plus dots, oblique hatching) where these amplitudes are great. Physical reasons for the occurrence of the increased amplitudes are different in these two cases.

In the left area (dots plus wavy hatching), we have an analogue of the amplification of acoustic–gravity waves propagating upwards in the atmosphere (a substantial increase in the amplitude of an acoustic–gravity wave can be achieved if the wave traverses a path many times as long as the scale height of the atmosphere). If an initial QAG perturbation is present in the cathode portion of the channel then, after a lapse of time, a pronounced anodal burst of intense small-scale irregular fluctuations takes place. Thus the left area corresponds to the flow regimes that appear to be unstable against anodal burst. As we know, the anodal burst is a phenomena associated with the properties of plasma media as such (Sec. 3).

In the right area of the parameter plane, the electrodes significantly affect the QAG waves in the plasma channel. Increased values of the electric current component normal to the electrode are characteristic of the neighbourhood of the boundary of this area. There the current-exchange instability manifests itself. The transition to the instability is sharper at the lower area boundary $\xi = \xi^{\mathrm{I}}(\nu)$. We note that the flow $\Pi = \Pi^0 + \tilde{\Pi}$ is here non-uniform in the transverse direction, and greater gradients are present near the anode. However, this non-uniformity is less pronounced than near the boundary of the left area, where the values of S are greater.

It seems likely that our results are of more general meaning. Thus Brushlinskiĭ and Morozov (1974) noted that small-scale oscillations can be considered a localized phenomenon and, since axisymmetric plasma flows with an azimuthal magnetic field do not differ locally from planar flows crossing the magnetic field, small-scale oscillations should behave similarly in both cases. Indeed, as we repeatedly saw above, there is a close similarity between the results of Brushlinskiĭ and Morozov (1974), who studied such axisymmetric flows numerically, and the results of our analytical investigation of planar flows.

Whereas the gliding of the current along the anode is a characteristic feature of a steady Hall flow, the formation of an electric current loop at the anode was regarded by Brushlinskiĭ and Morozov (1974) as a precursor of the transition to a non-steady-state regime at $\xi = \xi_{\mathrm{cr}}$. Since the formation of the current loop indicates a more active exchange of currents between the plasma and the electrode, I believe that it is the current-exchange instability of QAG waves that is responsible for the

https://doi.org/10.1017/S0022377899007606 Published online by Cambridge University Press

unstable regimes that were observed in the numerical experiments to set in after the formation of the current loop. This is supported by fact that the formula (1.1) used by Brushlinskiĭ and Morozov (1974) to approximate their numerically determined values ξ_{cr} coincides up to a geometric factor with our analytical formula (4.33) for the curve $\xi^{I}(\nu)$, which delimits the current-exchange-instability region (see Fig. 6). (This geometric factor can formally be obtained for Brushlinskiĭ's and Morozov's case of finite-width channels by putting $\delta = 1$ in (4.33); in this case, $\xi^{I}(\nu)$ proves to be three times greater than ξ_{cr} determined by (1.1).)

We note, however (see Sec. 1), that the phenomenon of anode explosion as described by Brushlinskiĭ and Morozov (1974) includes features of both the current-exchange instability and the anodal burst. The lack of distinction between these two phenomena in their study could be due to the procedure of the numerical experiments. Indeed, let us note that in these experiments, at a given ν, the value of ξ was successively increased from one run to another. At a certain stage, the flow became unstable because of either the anodal burst (for smaller ν values) or the current-exchange instability (for greater ν values) – cf. Fig. 6. These two phenomena could be perceived as a single process and described by the approximate curve (1.1). Figure 6 demonstrates the existence of steady solutions above the similar curve of (1.1) in our case, the stable region thus being more extensive than inferred from the numerical simulations.

It is also possible that the differences between the numerical and analytical results noted for smaller ν and ξ are related to differences in the flow structure between the two models – the axisymmetric and the planar one – that are present in the case of small ν. The simulations were carried out for channels with perfectly conducting, solid electrodes. This implies that the electric current is transverse to the Hall plasma flow only at sufficiently large ν. As $\nu \to 0$, however, a boundary layer with a large longitudinal current is formed near the electrode. It is the fashion, in order to avoid this effect, to make the electrodes sectioned (Morozov and Solov'ev 1964). In the problem addressed in our work, the electrodes are considered to be sectioned and the current is virtually transverse to the plasma flow even for small ν. In the analytical treatment of a problem more similar to our (but for $\nu \ll \delta^2$, whereas here $\nu \gg \delta/c, c \ll 1$), performed by Morozov and Shubin (1965) for the steady-state flow between sectioned electrodes, nothing was said about the existence of any forbidden range of ξ. This agrees indirectly with our conclusions.

8. General sense of the gamma factor and physical meaning of the restrictions imposed on the parameters

Of special concern is the factor $\gamma(x, y)$. We introduced it formally, seeking the solution Π in the form (2.14). However, this dimensionless quantity seems to be of fundamental significance for the theory of stationary (and nearly stationary) flows of Hall plasmas. It will now be shown that the factor γ (like the Reynolds number and other similarity criteria) can be found directly from the structure of the RHMHD equations for a planar flow (2.9)–(2.13) across a magnetic field; in so doing, it is not necessary to impose any restriction on the parameters or on the distribution of physical values throughout the flow. Thus let us now remove all of the restrictions introduced above and take a fresh look at the original equations (2.9)–(2.13).

https://doi.org/10.1017/S0022377899007606 Published online by Cambridge University Press

There are reasons to believe that the specific properties of Hall plasma flows originate from the particular features of the process of magnetic field generation in Hall plasma media. Here, as can be seen from the magnetic induction equation (2.12), the magnetic field can be generated not only by maintained motion of the conducting medium across the magnetic field (as is the case in ordinary non-Hall conductors), but also by a maintained medium-density gradient directed transverse to the magnetic field gradient ∇H.

With the use of (2.10), the equation of magnetic induction (2.12) can be rewritten in the form

$$\frac{\partial \mathbf{H}}{\partial t} = \nu \nabla^2 \mathbf{H} + \nabla \times (\mathbf{v} \times \mathbf{H}) + \frac{\xi}{c^2} \frac{H}{\rho} \frac{d\mathbf{v}}{dt} \times \nabla H.$$

We note that magnetic-field generation due to the Hall effect results in changes of the magnetic field in precisely those regions where the gradient ∇H transverse to the flow acceleration is already present. We investigate the case where such a generation process is sufficiently intense. This means that there is a tendency for progressively smaller scales to arise in the distributions of physical quantities in the direction normal to the flow acceleration. Accordingly, dissipation becomes progressively more significant. As a consequence, equilibrium between magnetic field generation due to the Hall effect and dissipation should be established at a sufficiently small spatial scale.

We shall now see that the magnitude of this limiting scale is of the order of γ^{-1}, and therefore the factor γ shows up as the characteristic of the sharp transverse inhomogeneity occurring in the stationary flow of a resistive Hall plasma in a channel. To show this, let us consider a stationary flow of such a kind where

$$0 = \nu \nabla^2 \mathbf{H} + \nabla \times (\mathbf{v} \times \mathbf{H}) + \frac{\xi}{c^2} \frac{H}{\rho} \mathbf{w} \times \nabla H \tag{8.1}$$

(here $\mathbf{w} = (\mathbf{v} \cdot \nabla)\mathbf{v}$).

We introduce a local Cartesian coordinate system (p, η) with stream-aligned p axis and transversely directed η axis (from the anode to the cathode), whose origin is at a certain point (x, y) that we denote as (0,0). Correspondingly, the velocity component v_η is equal to zero at the local coordinate origin and small in its vicinity. This gives $(\mathbf{v} \cdot \nabla)v_\eta \ll (\mathbf{v} \cdot \nabla)v_p$ or $w_\eta \ll w_p$ near the point (0,0).

In addition, since the transverse scale is small ($l_\eta \to 0$), we have $\partial H/\partial p \ll \partial H/\partial \eta$, and the Hall term in (8.1) proves to be equal to

$$B = \frac{\xi}{c^2} w_p \frac{H}{\rho} \frac{\partial H}{\partial \eta}. \tag{8.2}$$

Here we see that it is the longitudinal acceleration of the Hall plasma that gives rise to the studied effect of the generation of the small-l_η magnetic field. In other words, the *longitudinal* acceleration of the Hall plasma flow results in a strong *transverse* non-uniformity of the magnetic field or in the presence of an enhanced longitudinal electric current.

We now compare the Hall term B of (8.1) at a fixed value of ξ with the 'convective' term

$$[\nabla \times (\mathbf{v} \times \mathbf{H})]_z = -\frac{\partial}{\partial p}(v_p H) - \frac{\partial}{\partial \eta}(v_\eta H). \tag{8.3}$$

The first term can easily be estimated if, in the expression (8.2) for B, we replace the acceleration w_p by its part $v_p(\partial v_p/\partial p) \sim v_p^2/l_p$ (where $l_p \lesssim 1$ is the characteristic

https://doi.org/10.1017/S0022377899007606 Published online by Cambridge University Press

non-dimensional longitudinal scale; note that $l_p \gg l_\eta$). To estimate the second term on the right-hand side of (8.3), we replace w_p in the expression (8.2) by its other part $v_\eta(\partial v_p/\partial\eta)$. It then becomes evident that the ratio of the convective term to the Hall term in (8.1) does not exceed

$$l_\eta \frac{c^2}{\xi}\frac{\rho}{Hv_p}.$$

We restrict our consideration to channels in which the gasdynamic acceleration is not too strong in comparison with the magnetic acceleration, assuming that $\beta \lesssim 1$ (or, equivalently, $c^2 \lesssim 1$). Then the convective term proves to be negligible. Hence (8.1) acquires the form

$$\frac{\partial j_p}{\partial\eta} + \frac{\xi}{\nu c^2}\frac{H}{\rho} w_p j_p = 0, \tag{8.4}$$

where $j_p = \partial H/\partial\eta$ is the longitudinal component of the electric current. Thus, finally, we infer that the sought-for small transverse scale l_η of the Hall plasma flow is equal to γ^{-1}, where

$$\gamma(x,y) = \frac{\xi}{\nu c^2}\frac{H}{\rho} w_p. \tag{8.5}$$

This permits us to draw several useful conclusions.

(i) The inequality $\gamma \gg 1$ is a necessary condition for the existence of a stationary Hall plasma flow with a sharp transverse non-uniformity.

(ii) We find, making use of the Euler equation (2.10), that

$$\gamma(x,y) = -\frac{\xi}{\nu}\frac{H}{(\rho)^2}\frac{\partial}{\partial p}\left(\rho + \frac{H^2}{2c^2}\right). \tag{8.6}$$

Hence the non-uniformity of the stationary Hall plasma flow is stronger, the greater ξ and the smaller $\beta = 2c^2$ and ν. Thus, in channels with a significant gasdynamic acceleration, a very large value of $\xi/\nu = \omega_e\tau_e$ is necessary for the Hall effect to manifest itself in the flow, whereas this value may be small for regimes of magnetic acceleration of plasma ($\beta \ll 1$).

(iii) The flow is most strongly influenced by the Hall effect in the vicinity of the point where the product of H/ρ by the longitudinal acceleration w_p reaches its maximum.

(iv) The structure revealed in the flow is always of fixed polarity in the following sense: for accelerating channels ($w_p > 0$), the value $|j_p|$ always increases in the anode direction.

(v) As we saw, the strong transverse non-uniformity of the Hall plasma flow is due to plasma acceleration along the channel. Basically, the longitudinal acceleration w_p^0 is in essence determined by the conditions at the inlet and outlet of the channel, the magnetic field H^0 being created by the electric current j^0 directed predominantly across the channel, from the anode to the cathode. According to (8.4), which is 'linear' with respect to j_p, we should expect a sharp non-uniformity to manifest itself in the distribution of the small longitudinal

https://doi.org/10.1017/S0022377899007606 Published online by Cambridge University Press

current $\tilde{j}_p$, if the values of the constant parameters ξ, ν, and β are such that

$$\gamma(x,y) = \frac{\xi}{\nu c^2}\frac{H^0}{\rho^0} w_p^0 \gg 1. \tag{8.7}$$

Then the non-stationary disturbances associated with the small longitudinal current $\tilde{j}_p$ can also be classified. Indeed, by juxtaposing the left-hand side of (8.4) to $\partial\tilde{H}/\partial t$, we can estimate the characteristic time $t_{\rm mag} \sim \gamma^{-2}\nu^{-1}$ of the magnetic field variation. The time of gasdynamic response to magnetic pressure variations is $t_{\rm gas} \sim \gamma^{-1}/c$. For $\xi \ll c^3$, we have $t_{\rm gas} \ll t_{\rm mag}$, and the gasdynamic quantities can be considered quasistationary with respect to the time-dependent magnetic field. On the contrary, if $\xi \gg c^3$, we have $t_{\rm gas} \gg t_{\rm mag}$. When this takes place, the magnetic field comes into conformity with variable gasdynamic quantities in a very short time, and thus behaves as a quasistationary quantity. In this case, the plasma perturbations appear to be of gasdynamic nature.

Owing to the smallness of l_η, the properties established in this section for planar flows should have analogues in axisymmetric resistive Hall plasma flows with an azimuthal magnetic field. The studies of Brushlinskiĭ and Morozov (1974) (Sec. 1) have revealed such flow properties as especially pronounced appearance of the transverse non-uniformity in the distribution of the longitudinal component of the electric currents, the features of the dependence of the flow on the parameters pointed out in (ii), and the presence of the near-anode structure described in (iv).

In view of these results, we can now glance again, from a more general standpoint, at the QAG-wave solutions obtained in Secs 3–6. The factor γ determined by (8.6) acquires the form (2.15) owing to the inequality (2.17). The relation $\delta \ll 1$, which is a consequence of (2.19) and (2.17), allows one to extend the stationary local equation (8.4) to the whole flow region and thus describe the steady anode jump. The use of the relation $\xi \gg c$ in the condition (2.19) allows us to consider an (unsteady) acoustic regime. Correspondingly, the magnetic field is found to satisfy the quasistationary equation (3.9) for the magnetic induction. The quantity $\tilde{j}_x$, which is most strongly affected by the Hall effect, turns out to be proportional to $\tilde{\rho}$. Then the y component of the Lorentz force $\mathbf{j}\times\mathbf{H}$ in the Euler equation plays the role of a mass force, and effective gravity arises to produce QAG waves.

9. Conclusions

As we have seen, the Hall effect imparts unusual properties to a plasma flow crossing a magnetic field. If the values of the parameters ξ, ν and $\beta = 2c^2$ lead, according to (8.6), to very large values of $\gamma(x,y)$, a sharp transverse non-uniformity in the stationary Hall plasma flow proves to be governed by the longitudinal acceleration w_p of the flow (see Sec. 7). The most significant cross-gradients are localized near the anode.

If, in addition, $\xi \gg [(\beta/2)^3]^{1/2}$, then in time-dependent regimes the magnetic field quickly comes to conformity with the gasdynamic variables, and thus becomes quasistationary. In these circumstances, the time evolution of the Hall-plasma flow appears as a gasdynamic process.

In Sec. 3, we solved the full set of RHMHD equations for the parameters obeying these conditions (together with the condition $\beta \ll 1$). The solution has the form

https://doi.org/10.1017/S0022377899007606 Published online by Cambridge University Press

$\Pi = \Pi^0(x, y) + \tilde{\Pi}(x, y, t)$, where Π^0 is a known, rather arbitrary, stationary flow with $v_y^0/v_x^0 \sim \delta \ll 1$, relatively uniform in the y direction (see (2.16) and (3.6)), and its time-dependent perturbation $\tilde{\Pi}$ exhibits strong transverse non-uniformity with the spatial scale γ^{-1}. Indeed, the time evolution of $\tilde{\Pi}$ has a gasdynamic character, and the perturbation presents itself as an analogue of acoustic–gravity waves in the atmosphere. We call such plasma waves quasi-acoustic–gravity (QAG) waves.

The effective gravity force is produced by the magnetic field, and the 'gravitational' acceleration is equal to $c^2\gamma$, i.e. proportional to ξ/ν (or, equivalently, to $\omega_e\tau_e$). The phenomenon of effective gravity arises in a wide range of the parameters ξ and ν. In particular, it is possible at small values of $\omega_e\tau_e$.

QAG waves can also arise in a plasma channel where plasma flows between conducting sectioned electrodes (Secs 4–6). Given β and ν, if ξ is outside the interval $\xi^{\mathrm{I}}(\beta, \nu) < \xi < \xi^{\mathrm{II}}(\beta, \nu)$ determined by (4.33) and (4.34), free QAG oscillations occur (Figs 1, 2 and 6). The system of standing density waves includes a steady-state mode as well as a superposition of rapid harmonic oscillations, their amplitudes being maximum near the anode (see (5.8)). The solution proves to be determined by only one parameter, the ratio $S(x) = s(x)\gamma(x)$ of the channel depth s to the characteristic scale $l_y = \gamma^{-1}$ of the transverse non-uniformity. This solution is strongly S-dependent.

The Hall plasma flow exhibits the following peculiar features if S is very large.

(a) The distribution of the zeroth mode of $\tilde{\rho}$ over the cross-section assumes the form of a steady-state 'anodal jump' because a very large gradient transverse to the flow is present at the anode. It is in this anodal-jump layer that the electric current acquires a longitudinal component $\tilde{j}_x$.

(b) A perturbation initially localized near the cathode subsequently travels to the anode, forming a 'cathode' wave with a strongly increasing amplitude. After a lapse of time, this results in an anodal burst represented by intense irregular fluctuations with the maximum amplitudes in the anode zone of the channel.

(c) If at $t = 0$ the perturbation is mainly localized in the anodal portion of the channel (but does not coincide with the zeroth mode) then the anodal-jump pattern alternates in time with the initial state, and the pulsating-anodal-jump regime takes place. It persists the longer, the larger is S. Ultimately, this regime terminates abruptly owing to the breakdown of the perturbation into separate modes. If the initial perturbation (possibly weak) is also present in the cathode zone of the channel, the termination of the pulsating-anodal-jump regime has the character of an anodal burst.

(d) In all anodal-jump regimes (both steady and pulsatory), the transverse component of the velocity is either zero (in a steady jump) or small, whereas the longitudinal component $\tilde{v}_x$ turns out to be non-zero in the anodal-jump layer, increasing with time. Therefore, a narrow jet can eventually be formed in this thin layer if a pulsatory regime arises, the magnitude of $\tilde{v}_{x0}$ becoming significant.

(e) As ξ approaches $\xi^{\mathrm{I}}(\nu, \beta) = (\nu/\delta)^{1/2}(\beta/2)^{1/4}$ from below or $\xi^{\mathrm{II}}(\nu, \beta) = \beta\nu/2\delta$ from above, the listed properties of resistive Hall-plasma flows are modified (Sec. 6). Then the electric current component normal to the electrode increases. Owing to the interaction between the free QAG oscillations and the currents induced

https://doi.org/10.1017/S0022377899007606 Published online by Cambridge University Press

by them in the channel walls, a current-exchange instability develops. The stationary flow (the sum of the background flow and the steady-state anodal jump) ceases to exist, and a non-stationary regime with growing fluctuations sets in. This growth is especially rapid in the case of ξ approaching $\xi^{\mathrm{I}}(\nu, \beta)$ from below.

It seems likely that the results obtained for the planar geometry are of more general meaning. Since axisymmetric plasma flows with an azimuthal magnetic field do not differ locally from planar flows across the magnetic field, small-scale QAG waves should behave in the same way in either geometric class of flows.

I believe that the loss of stability by a steady flow due to both the anodal burst and the current-exchange instability has earlier been interpreted as an anode explosion in the numerical simulations of axisymmetric flows with an azimuthal magnetic field (see Sec. 1). In particular, a similarity between the formula (1.1) for $\xi = \xi_{\mathrm{cr}}(\nu, \beta)$ obtained by computations and our analytical expression (4.33) for $\xi = \xi^{\mathrm{I}}(\nu, \beta)$ also counts in favour of such an identification of phenomena. Note that in extending our analytical results for the planar geometry to the case of the axisymmetric geometry, one can expect the region of stable RHMHD flows to be wider than was thought earlier on the basis of the numerical investigation of Brushlinskiĭ and Morozov (1974)

Well-established plasma flows are desirable in many cases, and have been extensively studied in laboratories. The effective gravity revealed here arises in quasi-stationary regimes. Therefore the above-listed features of Hall plasma flows, which are related to QAG waves, should frequently be encountered in laboratory practice.

However, it is important to keep in mind that only in the case of the planar geometry does the gliding of the electric current near the electrode testify to the fact that the plasma flow is influenced by the Hall effect. In axisymmetric channels, the current can also glide in the absence of the Hall effect. This phenomenon is of a convective nature and the condition for its appearance is $\beta > 1$, which implies the predominance of the gasdynamic acceleration over the magnetic one (Alekseeva and Solov'ev 1964). The convective effect manifests itself in a variety of experiments (Morozov and Solov'ev 1974; Brushlinskiĭ and Morozov 1974; Garkusha et al. 1992). In contrast, the current gliding due to Hall effect is more pronounced for $\beta < 1$.

Acknowledgements

The author is grateful to the late L. S. Solov'ev and the late B. A. Tverskoĭ as well as to A. V. Getling for valuable discussions, and additionally to A. V. Getling for his indispensable participation in this work.

References

Alekseeva, L. M. and Solov'ev, L. S. 1964 *Prikl. Mat. Mekh.* **28**(6), 987–995.

Alekseeva, L. M. 1979 *Dokl. Akad. Nauk SSSR* **248**(4), 826–828.

Alekseeva, L. M. 1980 *Pis'ma Zh. Tekhn. Fiz.* **6**(21), 1310–1312 [Engl. transl. *Soviet Tech. Phys. Lett.* **6**, 561 (1980)].

Alekseeva, L. M. 1989 *Pis'ma Zh. Tekhn. Fiz.* **15**(10), 1–4 [Engl. transl. *Soviet Tech. Phys. Lett.* **15**, 371 (1989)].

Alekseeva, L. M. 1990 *Dokl. Akad. Nauk SSSR* **310**(3), 567–571 [Engl. transl. *Soviet Phys. Dokl.* **35**, 51 (1990)].

Alekseeva, L. M. 1991 *Pis'ma Zh. Tekhn. Fiz.* **17**(13), 6–10 [Engl. transl. *Soviet Tech. Phys. Lett.* **17**, 461 (1991)].

https://doi.org/10.1017/S0022377899007606 Published online by Cambridge University Press

Alekseeva, L. M. 1992a *Zh. Tekhn. Fiz.* **62**(2), 64–73 [Engl. transl. *Soviet Phys. Tech. Phys.* **37**(2), 146–151 (1992)].

Alekseeva, L. M. 1992b *Zh. Tekhn. Fiz.* **62**(2), 74–83 [Engl. transl. *Soviet Phys. Tech. Phys.* **37**(2), 152–157 (1992)].

Alekseeva, L. M. 1993 *Pis'ma Zh. Tekhn. Fiz.* **19**(5), 34–38 [Engl. transl. *Soviet Tech. Phys. Lett.* **19**(3), 145–147 (1993)].

Alekseeva, L. M. 1994a *Pis'ma Zh. Tekhn. Fiz.* **20**(5), 1–8 [Engl. transl. *Tech. Phys. Lett.* **20**(3), 175–177 (1994)].

Alekseeva, L. M. 1994b *Pis'ma Zh. Tekhn. Fiz.* **20**(12), 83–90 [Engl. transl. *Tech. Phys. Lett.* **20**(6), 511–514 (1994)].

Alekseeva, L. M. 1996 In: *Proceedings of 12th International Conference on Magnetohydrodynamic Electrical Power Generation, Yokohama, Japan, October 15–18, 1996*, Vol. 2, pp. 595–602.

Brushlinskiĭ, K. V. and Morozov, A. I. 1974 In: *Voprosy teorii plazmy*, Vol. 8 (ed. M. A. Leontovich), pp. 88–163 Atomizdat, Moscow [Engl. transl. *Reviews of Plasma Physics*, Vol. 8, Consultants Bureau, New York 1980].

Brushlinskiĭ, K. V., Morozov, A. I. and Savel'ev, V. V. 1979 In: *Dvumernye chislennye modeli plazmy* (Two-Dimensional Numerical Models of Plasmas), pp. 7–66. Inst. Prikl. Mat. Akad. Nauk SSSR, Moscow.

Garkusha, I. E., Morozov, A. I., Solyakov, D. G., Tereshin, V. I. and Chebotarev, V. Z. 1992 *Fiz. Plazmy* **18**(11), 1379–1384.

Gordeev, A. V., Kingsep, A. S. and Rudakov, L. I. 1994 *Phys. Rep.* **243**, 215–315.

Hines, C. O. 1960 *Can. J. Phys.* **38**, 1441–1471.

Holm, D. 1987 *Phys. Fluids* **30**, 1310–1322.

Huba, J. D. 1995 *Phys. Plasmas* **2**, 2504–2513.

Lamb H. 1932 *Hydrodynamics*, 6th edn. Cambridge University Press.

Morozov, A. I. and Shubin, A. P. 1965 *Teplofiz. Vys. Temp.* **3**(6), 826–837.

Morozov, A. I. and Solov'ev, L. S. 1964 *Zh. Tekhn. Fiz.* **34**(7), 1141–1153.

Morozov, A. I. and Solov'ev, L. S. 1974 In: *Voprosy teorii plazmy*, Vol. 8 (ed. M. A. Leontovich), pp. 3–87. Atomizdat, Moscow [Engl. transl. *Reviews of Plasma Physics*, Vol. 8, p. 1. Consultants Bureau, New York (1980)].

Rosenau, P., Tataronis, J. A. and Conn, G. 1979 *J. Plasma Physics* **21**, 385–399.

Solov'ev, L. S. 1963 In: *Voprosy teorii plazmy*, Vol. 3 (ed. M. A. Leontovich), pp. 245–289. Gosatomizdat, Moscow [Engl. transl. *Reviews of Plasma Physics*, Vol. 3, p. 1. Consultants Bureau, New York (1967)].

Tereshin, V. I., Voloshko, A. Yu., Voznyi, V. I., Garkusha, I. E., Zolotukhin, A. V. et al. 1990 In: *Ionnye inzhektory i plazmennye uskoriteli* (Ion Injectors and Plasma Accelerators) (ed. A. I. Morozov and N. N. Semashko), pp. 106–123. Energoatomizdat, Moscow.

Zimin, A. M. and Morozov, A. I. 1995 *Fiz. Plazmy* **21**(2), 126–131.

https://doi.org/10.1017/S0022377899007606 Published online by Cambridge University Press